The Astrophysical Journal, 719:1969–1983, 2010 August 20 doi:10.1088/0004-637X/719/2/1969

THE RISE AND FALL OF PASSIVE DISK GALAXIES: MORPHOLOGICAL EVOLUTION ALONG THE RED SEQUENCE REVEALED BY COSMOS

Kevin Bundy[1,13], Claudia Scarlata[2], C. M. Carollo[3], Richard S. Ellis[4], Niv Drory[5], Philip Hopkins[1], Mara Salvato[4,10], Alexie Leauthaud[6,12], Anton M. Koekemoer[7], Norman Murray[9], Olivier Ilbert[8], Pascal Oesch[3], Chung-Pei Ma[1], Peter Capak[2], Lucia Pozzetti[11], and Nick Scoville[4]

[1] Astronomy Department, University of California, Berkeley, CA 94705, USA
[2] Spitzer Science Center, California Institute of Technology, 314-6, Pasadena, CA 91125, USA
[3] Institute for Astronomy, ETH Zurich, 8092 Zurich, Switzerland
[4] Astronomy Department, California Institute of Technology, Pasadena, CA 91125, USA
[5] Max-Planck Institut fur extraterrestrische Physik, Giessenbachstrashe, 85748 Garching, Germany
[6] Physics Division, Lawrence Berkeley National Laboratory, 1 Cyclotron Road, Berkeley, CA 94720, USA
[7] Space Telescope Science Institute, Baltimore, MD 21218, USA
[8] Laboratoire d'Astrophysique de Marseille, BP 8, Traverse du Siphon, 13376 Marseille Cedex 12, France
[9] Canadian Institute for Theoretical Astrophysics, 60 St George Street, University of Toronto, ON M5S 3H8, Canada
[10] Max Planck Institut fuer Plasma Physics and Excellence Cluster Boltzmannstrasse 2, Garching 85748, Germany
[11] Osservatorio Astronomico di Bologna, Via Ranzani, 1, I-40127 Bologna, Italy
[12] Berkeley Center for Cosmological Physics, University of California, Berkeley, CA 94720, USA
Received 2009 December 5; accepted 2010 June 26; published 2010 August 4

ABSTRACT

The increasing abundance of passive "red-sequence" galaxies since $z \sim 1$–2 is mirrored by a coincident rise in the number of galaxies with spheroidal morphologies. In this paper, however, we show in detail, that, the correspondence between galaxy morphology and color is not perfect, providing insight into the physical origin of this evolution. Using the COSMOS survey, we study a significant population of red-sequence galaxies with disk-like morphologies. These passive disks typically have Sa–Sb morphological types with large bulges, but they are not confined to dense environments. They represent nearly one-half of all red-sequence galaxies and dominate at lower masses ($\lesssim 10^{10} M_{\odot}$) where they are increasingly disk-dominated. As a function of time, the abundance of passive disks with $M_* \lesssim 10^{11} M_{\odot}$ increases, but not as fast as red-sequence spheroidals in the same mass range. At higher mass, the passive disk population has declined since $z \sim 1$, likely because they transform into spheroidals. Based on these trends, we estimate that as much as 60% of galaxies transitioning onto the red sequence evolve through a passive disk phase. The origin of passive disks therefore has broad implications for our understanding of how star formation shuts down. Because passive disks tend to be more bulge-dominated than their star-forming counterparts, a simple fading of blue disks does not fully explain their origin. We explore the strengths and weaknesses of several more sophisticated explanations, including environmental effects, internal stabilization, and disk regrowth during gas-rich mergers. While previous work has sought to explain color and morphological transformations with a single process, these observations open the way to new insight by highlighting the fact that galaxy evolution may actually proceed through several separate stages.

Key words: galaxies: evolution – galaxies: formation

Online-only material: color figures

1. INTRODUCTION

It has long been known that nearby galaxies roughly fall into two categories: (1) systems with prominent disks often exhibiting spiral structure and ongoing star formation and (2) galaxies dominated by a spheroidal morphology—the most extreme being ellipticals—and harboring little if any star formation. With the advent of large galaxy surveys like the Sloan Digital Sky Survey (SDSS) it had been possible to quantify the bimodal nature of the local population both in terms of morphology and star formation as a function of what appears to be the best observationally accessible variable for separating the two populations, the galaxy's stellar mass (M_*; Bell et al. 2003; Kauffmann et al. 2003; Baldry et al. 2004; Balogh et al. 2004). The bimodal nature of the galaxy population is apparent to $z \sim 1$ (Bell et al. 2004) and beyond (e.g., van Dokkum et al. 2006), but it is clear that the fraction of galaxies populating either side must evolve with time. Brinchmann & Ellis (2000) presented evidence for an increase since $z \sim 1$ in the global mass density of morphological spheroidals at the expense of star-forming irregulars, and Cowie et al. (1996) showed that increasingly *K*-band luminous and therefore more massive galaxies exhibit higher specific star formation rates (sSFRs) at early times.

A number of more recent studies have confirmed and extended these early results, using mass and luminosity functions to trace the evolution since $z \sim 2$ of the two populations as partitioned by the amount of star formation or the rest-frame color (Juneau et al. 2005; Bundy et al. 2006; Borch et al. 2006; Willmer et al. 2006; Brown et al. 2007; Ilbert et al. 2010; Mobasher et al. 2009) and as a function of morphological type (Bundy et al. 2005; Pannella et al. 2006; Franceschini et al. 2006; Scarlata et al. 2007b; Abraham et al. 2007; van der Wel et al. 2007; Ilbert et al. 2010; Pozzetti et al. 2009; Oesch et al. 2010). The importance of environmental density has also been studied (Bundy et al. 2006; Cucciati et al. 2006; Cooper et al. 2007; Capak et al. 2007a; van der Wel 2008; Pannella et al.

[13] Hubble Fellow.

2009; Tasca et al. 2009; Bolzonella et al. 2009). The emerging picture is one in which, beginning at the highest masses, galaxies transform from blue, star-forming, disk-dominated systems into red, bulge-dominated spheroidals in which star formation has been quenched. As time proceeds, this transformation process works its way down the mass function, driving the apparent downward shift in the bimodality mass scale.

Understanding the physical driver of this evolution has been a key challenge, leading to a search for a process capable of simultaneously shutting down star formation and turning disks into spheroidals. Morphological evolution has often been attributed to the "merger hypothesis" (Toomre 1977) in which galaxy mergers convert rotation-supported disks into pressure-supported spheroids. In a series of papers, Hopkins and collaborators demonstrate the feasibility of this idea through detailed simulations and link mergers with an explosive quasar or starburst phase that may heat or drive out cold gas in the spheroidal merger remnant, thereby quenching star formation (see Hopkins et al. 2008 and references therein). The idea that mergers quench star formation, at least in halos above a critical mass, $M_{\rm crit} \sim 10^{12} M_{\odot}$ (where the cooling time is longer than the dynamical time; see Dekel & Birnboim 2006), has also been implemented in semi-analytic models, in which supposedly spheroidal merger remnants are kept "red and dead" by so-called "radio mode" active galactic nucleus (AGN) feedback (Croton et al. 2006; Bower et al. 2006; Cattaneo et al. 2006; Somerville et al. 2008). Birnboim et al. (2007) argue against the need for mergers and AGN feedback, relying instead on the interplay between shock heating and cold flows in halos near $M_{\rm crit}$ (see also Dekel et al. 2009). Semi-analytic models based on this framework have needed to include some additional quenching tied to bulge growth after galaxy mergers to match the observed fraction of passive galaxies (Cattaneo et al. 2008).

One way to distinguish between these scenarios and gain insight into the transformation mechanisms at work is to test the link between quenching and morphological evolution by studying those galaxies whose morphological type places them on one side of the bimodality but whose star formation identifies them with the other. Star-forming blue ellipticals are one example (e.g., Schawinski et al. 2009; Kannappan et al. 2009; Ferreras et al. 2009; Brand et al. 2009) and are understood to be a combination of recent arrivals to the red sequence (Ruhland et al. 2009), bulge-dominated systems experiencing triggered star formation after minor mergers (Kaviraj et al. 2009) or, at low masses, the formation of new disks in gas-rich environments (Kannappan et al. 2009). The other possibility, namely, quenched or passive disk galaxies, is more challenging to explain because the shutdown of star formation must leave the disk in place. Yet examples in the local universe do exist. Lenticular or S0 galaxies are one example, although they typically live in galaxy clusters where interactions with the intercluster medium (e.g., ram pressure stripping; see Moran et al. 2007a) can remove the gas supply and shut down star formation. However, S0s have properties that do not depend on cluster density and a non-negligible fraction (∼8%) of nearby S0s are isolated, suggesting that not all S0s form as a result of living in dense environments (van den Bergh 2009). At slightly higher redshifts, $z \approx 0.1$, axis ratio distributions and Galaxy Zoo (GZ) morphologies have demonstrated an unmistakable population of red, disk-dominated galaxies that appear to live in the field and slightly overdense environments, but are not found solely in dense regions (Bamford et al. 2009; Masters et al. 2010; van der Wel et al. 2009). Finally, using the *Hubble Space Telescope* (*HST*) data in the Great Observatories Origins Deep Survey (GOODS) fields at $z \sim 1$, Bundy et al. (2006) compared color and morphologically classified mass functions to argue that quenching appeared to precede spheroid formation, finding hints of a red disk population at $z \sim 1$ (see also Pozzetti et al. 2009). Some examples of passive disks have even been found at $z \sim 2$ (Stockton et al. 2008).

The goal of this paper is to utilize the unprecedented size of the COSMOS field with its 1.64 deg^2 of *HST* imaging to revisit the question of red, passive disks in field environments and quantify their origin and evolution since $z \sim 1$. We argue that the behavior of this population presents a challenge to models that attribute morphological and color evolution to a single event, and may shed light on mechanisms that affect the galaxy population more broadly. This work follows on mass function studies of the COSMOS field as a function of color and morphological type by Ilbert et al. (2010), Pozzetti et al. (2009), Oesch et al. (2010), and Drory et al. (2009). Ilbert et al. (2010) specifically showed a broad connection in the behavior of morphologically early-type galaxies and those with passive stellar populations, but also presented evidence for an increasing fraction at high redshift of non-spheroidal morphologies among quenched systems—this is the starting point for the present study.

Throughout this paper, we use the AB magnitude system and adopt a standard cosmology with $H_0 = 70\ h_{70}$ km s^{-1} Mpc^{-1}, $\Omega_M = 0.3$, and $\Omega_\Lambda = 0.7$.

2. OBSERVATIONS

2.1. The COSMOS Field

The COSMOS field ($10^{\rm h}00^{\rm m}28\overset{\rm s}{.}6$, $+02^\circ12'21\overset{''}{.}0$) is the largest contiguous area (1.64 deg^2) imaged by the *HST* and is almost 20 times the size of the two GOODS fields combined. As such, it marks an unprecedented step forward in studies of the morphologies of distant ($z \sim 1$) galaxies at high resolution. Specifically for this work, COSMOS provides such large samples that we can statistically track evolving sub-samples of field galaxies defined by both rest-frame color *as well as* morphology as a function of M_* and redshift from $z \sim 1$ to $z \sim 0.1$.

A large team of scientists has assembled to collaborate on a wide range of topics using observations from the COSMOS field (for a review, see Scoville et al. 2007b). The primary data sets of interest for this work are the i_{814W} observations from the *HST* Advanced Camera for Surveys (ACS; Scoville et al. 2007a; Koekemoer et al. 2007), which provide morphological information, and the ground-based optical to near-IR photometry presented in detail in Capak et al. (2007b) and updated in Ilbert et al. (2009). As we discuss further below, the ground-based catalog provides the basis for high-precision photometric redshifts and a set of rest-frame colors that separate truly passive stellar populations from those that are actively star-forming but dusty.

We briefly review the relevant components of the ground-based catalog, referring to Capak et al. (2007b) and Ilbert et al. (2009) for details. The catalog includes u^*- and i^*-band imaging from Mega-Prime (Aune et al. 2003; Boulade et al. 2003) and was cross-referenced with K_s-band observations (McCracken et al. 2010) from the Wide-field InfraRed Camera (WIRCAM; Puget et al. 2004), both of which are instruments on the Canada–France–Hawaii Telescope (CFHT). The majority of photometric bands in the catalog were observed with the Subaru Telescope equipped with Suprime-Cam (Komiyama et al. 2003;

Table 1
Sample Statistics

z	All	Passive	Star-forming	Passive Early Disk	Passive Late Disk	Passive Extreme Disk
$0.2 < z < 0.4$	17210	2402	14808	755	380	30
$0.4 < z < 0.6$	16324	1744	14580	523	171	17
$0.6 < z < 0.8$	22253	2821	19432	883	261	36
$0.8 < z < 1.0$	25581	4075	21506	1282	356	81
$1.0 < z < 1.1$	6014	480	5534	160	42	5
$1.1 < z < 1.2$	14860	517	14343	165	28	5

filters $B_J, V_J, g^+, r^+, i^+, z^+$). The catalog was selected based on detections in the Subaru i^+ band and the seeing of the final mosaics is better than 1.″5 in all cases. Capak et al. (2007b) point-spread function (PSF) match all data, optimizing for photometry performed in 3″ diameter apertures. All of the optical bands have a 5σ point-source (3″ diameter aperture) depth of at least 25th magnitude (AB) with the K_s band limited to $K_s < 24$. Given these depths, the final sample completeness is determined mostly by the ACS data because morphological classification begins to degrade at magnitudes fainter than $i_{814W} \approx 24$. The *HST* ACS imaging is described in Scoville et al. (2007a) and Koekemoer et al. (2007), and is used only for morphological classification in this work. We use the Zurich Estimator of Structural Types (ZEST) morphology catalog (Scarlata et al. 2007a)—discussed further in Section 3.4—which is based on the ACS source catalog presented in Leauthaud et al. (2007) who estimate the ACS depth at $i_{814W} = 26.1$ for photometry of a 1″ galaxy.

2.2. The Primary Sample

In the analysis that follows, our primary sample is based on the *i*-selected catalog from Capak et al. (2007b). We impose magnitude limits of $K_s < 24$ and $i < 26.5$ and divide our sample into six redshift bins: [0.2–0.4), [0.4–0.6), [0.6–0.8), [0.8–1.0), [1.0–1.1), [1.1–1.2). Given the magnitude cuts, we estimate the mass completeness of each redshift bin by considering the observed magnitude of a maximal M_*/L stellar population model with solar metallicity, no dust, and a $\tau = 0.5$ Gyr burst of star formation that occurred at $z_{\rm form} = 5$. This exercise provides limits that roughly match the 80% completeness limits determined when deeper samples are available (Bundy et al. 2006), and in this case gives values of 8.8, 9.3, 9.7, 10.0, 10.1, and 10.2 in units of $\log M_*/M_\odot$.

In practice, morphological classification is not possible for every source down to the K_s- and *i*-band limits. This means that the effective M_* above which morphological samples are complete is higher than the full sample. These depend on the nature of the source, however, but can be easily defined with respect to the deeper $K_s < 24$ and $i < 26.5$ sample. We consider the morphological sample incomplete when the fraction of galaxies with a successful ZEST morphological classification (see Section 3.4) falls below 50% of the primary sample. We also limit the sample to ensure the robustness of ZEST classifications using ellipticity distributions tests (see Section 4.2). For each of the redshift bins defined above, we adopt mass limits of 9.7, 9.9, 10, 10.4, 10.5, and 10.8 in units of $\log M_*/M_\odot$. After removing stars and bright AGN, the number of galaxies in the primary sample in each redshift bin is listed in Table 1.

2.2.1. Cosmic Variance

While population studies using COSMOS data largely agree with previous work based on smaller fields (see Section 1), the sample or cosmic variance even in surveys covering a few square degrees represents a significant uncertainty that must be considered when interpreting our results (see Meneux et al. 2009). The largest effect is on the overall normalization of the total galaxy abundance (e.g., Bundy et al. 2006) although fractional abundance values are also affected. Stringer et al. (2009) use the variance gleaned from multiple mock light cones based on the Millennium Simulation to estimate the cosmic variance signal for a number of surveys, including COSMOS. From one redshift interval to another, they find typical abundance uncertainties of 0.2 dex. This estimate is consistent with the results in this work.

3. METHODS

3.1. Estimating Photometric Redshifts

While a spectroscopic survey, *z*COSMOS, is ongoing in the COSMOS field (Lilly et al. 2007), the large samples required for this work necessitate the use of photometric redshifts. We use the catalog of photo-*z*'s published by Ilbert et al. (2009) which are based on 30 bands of imaging in the COSMOS field. In addition to the observations mentioned in Section 2, these include UV bands from the *Galaxy Evolution Explorer* (*GALEX*), four mid-IR bands (3.6–8 μm) from the Infrared Array Camera (IRAC) on the *Spitzer Space Telescope*, *J*-band imaging from the Wide Field IR Camera (WFCAM) on the UK IR Telescope (UKIRT), and an additional 12 medium-band and two narrowband filters observed with Suprime-Cam on Subaru. This extended data set is described in detail by P. Capak et al. (2010, in preparation).

Redshift estimates were obtained with the *Le Phare*[14] code using templates drawn from Polletta et al. (2007). Ilbert et al. (2009) develop a novel technique that accounts for the contribution of emission line flux (especially important in the narrow and medium filter bands) to the spectral energy distributions (SEDs) of star-forming galaxies. This correction improves the photo-*z* precision by a factor of $\sim$2. When comparing to *z*COSMOS spectroscopic redshifts with $17.5 \leqslant i^+ \leqslant 22.5$, Ilbert et al. (2009) find a precision of $\sigma_{\Delta z}/(1+z) \approx 0.01$ after removing an outlier fraction that accounts for 0.6% of the comparison sample. They also compare to spec-*z*'s obtained with Keck DEIMOS (Faber et al. 2003) for a sample of very faint and 24 μm selected sources. At $i^+ \approx 25.5$ the uncertainties are estimated at $\sigma_{\Delta z}/(1+z) \approx 0.06$.

3.2. Estimating Stellar Masses

We use the Bayesian code described in Bundy et al. (2006) to estimate the current mass in stars of the galaxies in our sample. The observed SED of each galaxy is compared to a grid of 13,440 models from the Bruzual & Charlot (2003, hereafter BC03) population synthesis code that spans a range of metallicities,

[14] www.oamp.fr/people/arnouts/LE_PHARE.html

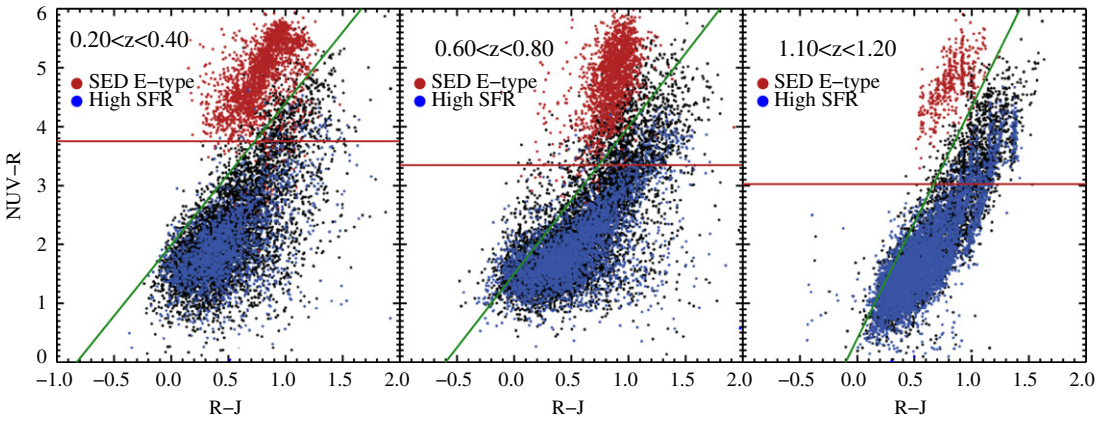

Figure 1. Rest-frame (NUV − R) vs. ($R - J$) color–color diagrams in three redshift bins selected to represent the full z-range of our sample ($0.2 < z < 1.2$). As shown by Williams et al. (2009), the addition of a near-IR filter helps break the degeneracy between dusty star-forming galaxies (red in NUV − R and red in $R - J$) and truly passive populations, which form a tight locus that is red in NUV − R but blue in $R - J$. The lines indicate the adopted color cuts. Red and blue colors indicate early and highly star-forming SED types, respectively, as identified by the photo-z fitting code of Ilbert et al. (2009).

(A color version of this figure is available in the online journal.)

star formation histories (parameterized as exponentials), ages, and dust content. No bursts are included in our models and only those models with ages (roughly) less than the cosmic age at each redshift are considered. We use a Chabrier initial mass function (IMF; Chabrier 2003) and assume a Hubble constant of 70 km s^{-1} Mpc^{-1}.

At each grid point, the K_s-band M_*/L_K ratios, inferred M_*, and probability that the model matches the observed SED is stored. This probability is marginalized over the grid, giving the stellar mass probability distribution, the median of which is taken as the final estimate of M_*. The width of the distribution provides the uncertainty which is typically 0.1–0.2 dex. This is added in quadrature to the K_s-band magnitude uncertainty to determine the final error on M_*. Stellar mass estimates for galaxies with photo-z's also suffer from the uncertainty in luminosity distance introduced by the photo-z error and the possibility of catastrophically wrong redshift information (Bundy et al. 2005; Kitzbichler & White 2007).

More broadly, any stellar mass estimate suffers potential systematic errors[15] from uncertainties inherent in stellar population modeling and various required assumptions, such as the form of the IMF. Several papers have stressed the importance of treating thermally pulsating asymptotic giant branch stars (TP-AGBs; e.g., Maraston et al. 2006), an element that is missing in the Bruzual & Charlot (2003) models. The recent and thorough investigation of population synthesis modeling by Conroy et al. (2009), however, argues that M/L ratios estimated from BC03 are largely resistant to the uncertain contribution from TP-AGBs as well as other limitations of current models. A further test is provided in Drory et al. (2009) who compare mass functions computed using BC03 and BC07 stellar population codes and conclude that ∼20% differences in abundances can be introduced, especially for star-forming galaxies. It is also important to recognize that M_* estimates may be affected by unrecognized systematic uncertainties at the 0.1–0.2 dex level.

3.3. Excluding Dusty Red-sequence Galaxies

Because our goal in this paper is to study disk galaxies that have stopped forming stars, in this section we discuss the rest-frame galaxy colors we use to identify passive stellar populations. Previous work has often relied on a single rest-frame UV-optical color to select passive galaxies, but this technique leads to possible contamination from dusty star-formers (e.g., Yan et al. 2006). In this work, we make use of color–color diagrams that include rest-frame UV, optical, and near-IR colors, inspired by recent work showing how this approach separates dusty star-formers from truly passive populations (e.g., Pozzetti & Mannucci 2000; Labbé et al. 2005; Wuyts et al. 2007; Williams et al. 2009).

The utility of the rest-frame UV–optical–near-IR "bicolor" diagram for the COSMOS data set is illustrated in Figure 1 where we show interpolated rest-frame colors in various redshift bins using the following filter bands: the *GALEX* near-UV band (NUV), the Suprime-Cam r^+ band, which we label as R, and a generic J-band filter.[16] Rest-frame NUV- and R-band absolute magnitudes were estimated by Ilbert et al. (2009) during the SED fitting necessary for measuring photo-z's. To derive the rest-frame J-band absolute magnitudes needed for the NUV–R–J diagram, we used the `Kcorrect` software package (Blanton & Roweis 2007) and the full suite of photometry described in Section 2. The broad wavelength coverage of COSMOS ensures that the flux corresponding to a given rest-frame filter is well sampled. A similar diagram was discussed in Ilbert et al. (2010).

The upper left portion of each redshift panel in Figure 1 exhibits a relatively tight clump of galaxies that we associate with passive stellar populations. A sequence of star-forming galaxies is evident below and to the right of the clump in each panel. As a test, we have colored in red those galaxies with SEDs best fit by early "spectral" type templates, as determined by the photo-z code (this category includes types 1–8 in the COSMOS photo-z fits; see Ilbert et al. 2009). Highly star-forming templates are shown in blue. At most redshifts, the early-type SED designation overlaps well with the associated passive clump. Note that the location and orientation of the passive clump and star-forming sequence evolves somewhat given our choice of filters. In what follows, we will isolate passive clump galaxies (also referred to hereafter as the "red sequence") using a joint color cut that evolves accordingly and is indicated by the two lines in Figure 1. Recognizing that

[15] These are not included in our final error estimates.

[16] As this work was completed, J-band observations of the COSMOS field were obtained using the WFCAM on UKIRT which has a different filter response function than the generic J-band filter used here.

such color cuts are somewhat arbitrary, our goal is to evenly split the now meandering "green valley" that separates the two populations. We specify our thresholds in terms of the given filters because they correspond well to our observations and do a good job of making the passive clump distinct, although we acknowledge that a more general treatment would be valuable in future work. Still, we emphasize that adjusting the details of the cuts defined below has little effect on the analysis that follows.

The horizontal NUV − R color cut is tuned to the usual luminosity-dependent bimodality (e.g., Willmer et al. 2006) in this color and is defined as follows:

$$\mathrm{NUV} - R > 4.2(1+z)^{-0.43} - 0.2(M_K + 20), \quad (1)$$

where M_K is the rest-frame absolute K_s-band magnitude. Passive galaxies must also satisfy the following diagonal cut in Figure 1:

$$\mathrm{NUV} - R > C_1(z) + C_2(z)(R - J), \quad (2)$$

where the constants, C_1 and C_2, have been chosen by inspection in redshift bins of width 0.2 with central values of $z = [0.30, 0.50, 0.70, 0.85, 0.95, 1.10]$. They are given by $C_1(z) = [4.4, 4.2, 4.0, 3.9, 3.8, 4.2]$ and $C_2(z) = [2.41, 2.41, 2.5, 2.6, 3.0, 3.7]$. At $z \lesssim 0.6$ the combination of the color cuts above select 10%–20% more passive galaxies than those with early-type SED templates, many of them scattered between star-forming and passive sequences. At higher redshifts, however, the SED method appears to miss genuine galaxies in the passive clump, as many as 20% at $z \approx 1$. We note that our conclusions regarding passive disk galaxies are unchanged if we use the SED fits to define the passive population.

Finally, we have checked for obscured star formation among the passive population as indicated by MIPS 24 μm emission. We note that a significant fraction of 24 μm emission, especially among the passive population, might arise from AGNs (e.g., Fiore et al. 2008). In addition, among star-forming galaxies, the implied SFR from 24 μm emission must be added to that from the UV flux which will dominate the output luminosity from star formation in our sample (e.g., Noeske et al. 2007). As a result, our constraints on hidden star formation in passive galaxies compared to star-formers are upper limits. Using the morphological classifications defined below (grouping "early" and "late" disks together), our first test compares 3σ MIPS detection rates of passive versus star-forming disk galaxies. For $z > 1$, no passive disks are detected with MIPS while the detection rate among star-forming disks is roughly 10%. In our lowest redshift bin, $0.2 < z < 0.4$, 1% of passive disks are detected compared to 10% of star-formers. At redshifts in between, the highest detection rates of passive disks occur at $0.4 < z < 0.6$, where 5% are detected compared to 8% for star-forming disks. Considering the full redshift range, these numbers confirm that the color–color methodology described above does not lead to significant contamination from hidden star formation. However, given the small numbers of MIPS detections, it is not possible to compare 24 μm flux as a function of M_* or put constraints on the relative amount of SFR hidden among passive population but below the MIPS detection limits.

For this, we perform a stacking analysis of the MIPS data in bins of stellar mass (of width 0.5 dex) and in the redshift intervals used throughout (the minimum number of galaxies per bin is roughly 20). Using Rieke et al. (2009), we estimate mean sSFR given the stacked 24 μm emission. Across our ∼30 stacked bins, the average passive sSFR is roughly an order of magnitude less than the star-forming sSFR. In two bins this difference approaches a factor of 2, and in several other bins, there is no stacked MIPS detection for passive galaxies. We note that the IR/SFR calibrations become uncertain at low 24 μm luminosities below $\log L_{24}/L_\odot < 8.5$ and several of our bins reach this limit. With this caveat and again ignoring contributions from AGN, our stacking analysis provides a rough upper limit to the possible amount of hidden star formation (SF) in the average passive galaxy that corresponds to growth rates of 3%–5% in M_* per Gyr.

3.4. Morphological Classification

Understanding the morphological makeup of the galaxy population is crucial to our goals in this paper. Given the large samples (typically more than 10^5 galaxies) made possible by the COSMOS data, automated morphological classifiers figure prominently. It is well known, however, that techniques such as CAS (e.g., Conselice 2003) or Gini/M20 (see Abraham et al. 2007) often disagree when compared to visual morphologies and can differ from each other. Indeed, Ilbert et al. (2010) use two different classifiers—the Gini/M20 method described in Abraham et al. (2007) and a CAS-like technique used in Cassata et al. (2007)—to gauge the systematic uncertainty of broad categories such as "spheroidal" or "disk-like." Their analysis of the evolving distribution of morphologies in COSMOS from $z \sim 1$ serves as the basis for this work. We should also note that "wiki-morphologies" of the kind pioneered by GZ (Lintott et al. 2008) are an alternative way to obtain visual morphologies for large samples.

In this work, we are specifically interested in disk components living in passive galaxies. As such, the exact definitions of morphological type are less important than confidence in the ability of the chosen classifier to find disk-like structure even if embedded in bulge-dominated galaxies and, ideally, to parameterize the prominence of disks compared to an accompanying bulge component. The ZEST automated classifier satisfies these requirements and has also been trained to match visual classifications of local surveys. Our strategy is to adopt the ZEST classification in the COSMOS sample and test it both through visual inspection of COSMOS galaxies and an independent check of our results using visual morphologies determined in GOODS-N and published in Bundy et al. (2005).

3.4.1. The ZEST Automated Classifier

ZEST combines the power of a principle component (PC) analysis of nonparametric measures of galaxy structure with information from a parametric fit. Details are presented in Scarlata et al. (2007a) but we review the salient features here. The light concentration, asymmetry, Gini coefficient, second-order moment of the brightest 20% of the flux, M_{20}, and the ellipticity are input to a PC analysis which delivers eigenvectors (linear combinations of the input parameters) that maximize the observed sample variation, thereby allowing for a compression of the original parameter space. Only the first three PCs, PC_1, PC_2, and PC_3, are retained for further analysis because they contain the bulk of the sample variance. The PC_1–PC_2–PC_3 space defined by a training sample of 56,000 $i_{814W} < 24$ galaxies was divided into a three-dimensional grid. Every galaxy living in a given unit cube was visually inspected so that a broad morphological type could be assigned to that cube. A value of $T_{\mathrm{ZEST}} = 1$ corresponds to "elliptical," $T_{\mathrm{ZEST}} = 2$ to "disk," and $T_{\mathrm{ZEST}} = 3$ to "irregular." In the case of $T_{\mathrm{ZEST}} = 2$ (disk) cubes, the average value $\langle n \rangle$ from single-Sérsic fits for galaxies with

$i_{814W} < 22.5$ from Sargent et al. (2007) was used to establish a "bulge" parameter, B_{ZEST}, for each cube which was then applied to fainter magnitudes. Higher values of B_{ZEST} indicate smaller bulges and larger disks, with $B_{ZEST} = [0, 1, 2, 3]$ corresponding to Sérsic n ranges of $\langle n \rangle \geqslant 2.5, 1.25 \leqslant \langle n \rangle \leqslant 2.5, 0.75 \leqslant \langle n \rangle \leqslant 1.25$, and $0 \leqslant \langle n \rangle \leqslant 0.75$. In the analysis that follows, we consider three ZEST morphological types.

1. "Spheroidal" includes $T_{ZEST} = 1$ ellipticals as well as highly bulge-dominated S0-like systems with $T_{ZEST} = 2$ and $B_{ZEST} = 0$ ($\langle n \rangle \geqslant 2.5$).
2. "Early disks" are likely to host significant bulges and have $T_{ZEST} = 2$ and $B_{ZEST} = 1$ ($1.25 \leqslant \langle n \rangle < 2.5$).
3. "Late disks" likely have smaller bulges with $T_{ZEST} = 2$ and $B_{ZEST} = 2$ ($0.75 \leqslant \langle n \rangle < 1.25$).
4. "Extreme disks" have little to no bulge component with $T_{ZEST} = 2$ and $B_{ZEST} = 3$ ($0 \leqslant \langle n \rangle < 0.75$).

The ZEST morphologies were previously tested using a sample of 80 visually classified $z = 0$ galaxies drawn from the RC3 catalog (de Vaucouleurs et al. 1991; Frei et al. 1996). As shown in Figure 6 of Scarlata et al. (2007a), the ZEST classifications agree well with the published morphologies. Of relevance to the current work, galaxies with $T_{ZEST} = 2$ (disks) and $B_{ZEST} > 0$ are always associated with types later than S0 with no contamination from ellipticals. Of disks with $B_{ZEST} = 1$, 43% have published types between S0 and Sab and 57% have types Sb–Scd. Of disks with $B_{ZEST} = 2$, 5% are classified as S0–Sab, 45% as Sb–Scd, and 50% as Sd type and later.

At faint magnitudes the ZEST morphologies begin to break down, as discussed further in Scarlata et al. (2007a). This can be quantified by degrading the signal-to-noise ratio (S/N) of bright galaxies for which the morphology is well determined. Down to $i_{814W} = 22.5$ fewer than 10% experience any change in either T_{ZEST} or B_{ZEST} and those that do mostly lie near classification boundaries. Even when degraded to $i_{814W} = 24$, the effective limit for morphological classification, the fraction identified with their original morphological type is 65%. Because we will be interested in trends between morphology, mass, and redshift, it is important to note that at faint magnitudes, the ZEST morphologies are biased to later types. Scarlata et al. (2007a) estimate that at most 30% of early-type galaxies could be misclassified as disk or irregular type at the faintest magnitudes. We will show that this potential bias is smaller than the detected amount by which disks outnumber spheroidals at the faint ends of our sample. Furthermore, imposing brighter magnitude limits (e.g., $i_{814W} < 22.5$) to reduce the potential for poor classifications does not alter our basic conclusions.

3.5. Estimating Comoving Number Densities

We compute mass functions in this work using the V_{max} technique (Schmidt 1968). We weight galaxies by the maximum volume in which they would be detected within the K_s-band and i^+-band limits in a given redshift interval. In practice, our magnitude limits ($K < 24$ and $i^+ < 26.5$) impose restrictions only in the highest redshift bins ($z \gtrsim 1$) and at masses below the limit where morphological classification becomes difficult. For each host galaxy i in the redshift interval j, the value of V^i_{max} is given by the minimum redshift at which the galaxy would drop out of the sample

$$V^i_{max} = \int_{z_{low}}^{z_{high}} d\Omega \frac{dV}{dz} dz, \quad (3)$$

where $d\Omega$ is the solid angle subtended by the survey area, and dV/dz is the comoving volume element. The redshift limits are given as

$$z_{high} = \min\left(z^j_{max}, z^j_{K_{lim}}, z^j_{i_{lim}}\right) \quad (4)$$

$$z_{low} = z^j_{min}, \quad (5)$$

where the redshift interval, j, is defined by $[z^j_{min}, z^j_{max}]$, and $z^j_{K_{lim}}$ and $z^j_{i_{lim}}$ refer to the redshift at which the galaxy would still be detected below the K_s-band and i^+-band limits. We use the best-fit SED template as determined by the stellar mass estimator to calculate these values, thereby accounting for the K-corrections necessary to compute V_{max} values (no evolutionary correction is applied).

4. RESULTS

4.1. Morphological Makeup of the Red Sequence

Our main results are shown in Figures 2 and 3 which present the absolute mass function and fractional contribution of passive galaxies (which we refer to as the "red sequence") divided by ZEST morphological type into spheroidals, early disks, and late disks. The mass distributions of all red-sequence galaxies (red dashed line), all star-forming galaxies (blue dash-dotted line), and the full sample (black solid line) are also indicated. The statistical uncertainties are encoded by the width of the shaded regions. The sample (or cosmic) variance in COSMOS (see Section 2.2.1) is estimated at 0.2 dex and is likely responsible for the high apparent abundance values (especially for passive objects) in the $0.8 < z < 1.0$ bin, a feature seen in previous work (Ilbert et al. 2010; Drory et al. 2009; Pannella et al. 2009; Pozzetti et al. 2009). Extreme disks with passive colors are so rare that we do not plot them and for clarity we omit the morphological mass functions of star-forming galaxies. Though we do not show it, it is important to note that at low masses star-forming disks of all three types far outnumber passive disks, while at the highest masses they are roughly equal in absolute numbers. The 50% completeness of the ZEST morphological sample is indicated with vertical dotted lines in Figure 2 while data points below this limit are simply omitted in Figure 3. These limits are nearly identical to the 50% completeness limits that would be obtained imposing a brightness limit of $i_{814W} < 24$.

Figures 2 and 3 show that galaxies on the red sequence, even after removing those contaminated by dust, are remarkably diverse in their morphologies. This may have been missed in previous data sets that were limited to the highest masses where spheroidals do indeed dominate the red sequence. Thanks to the greater depth of the COSMOS photometry, the ZEST morphologies reveal a significant population of red-sequence galaxies at lower masses that appear to harbor disk components. These become prominent below a stellar mass scale that evolves downward with time from $(1–2) \times 10^{11} M_\odot$ at $z \approx 1.2$ to $\approx 10^{10} M_\odot$ at $z \approx 0.3$. Considering the full red sequence (defined by the mass range over which the fraction of passive galaxies is $f_{red} > 10\%$) we find that at every redshift, passive disks (early + late) are identified in as much as half of red-sequence galaxies and become dominant at the low-mass end. This increase in passive disks is robust to the maximum combined biases that could result from morphological classifications as well as cosmic variance. Dividing disks further into "early" and "late" depending on whether the average Sérsic $\langle n \rangle$ values are greater than or less than 1.25, we see that disk galaxies with

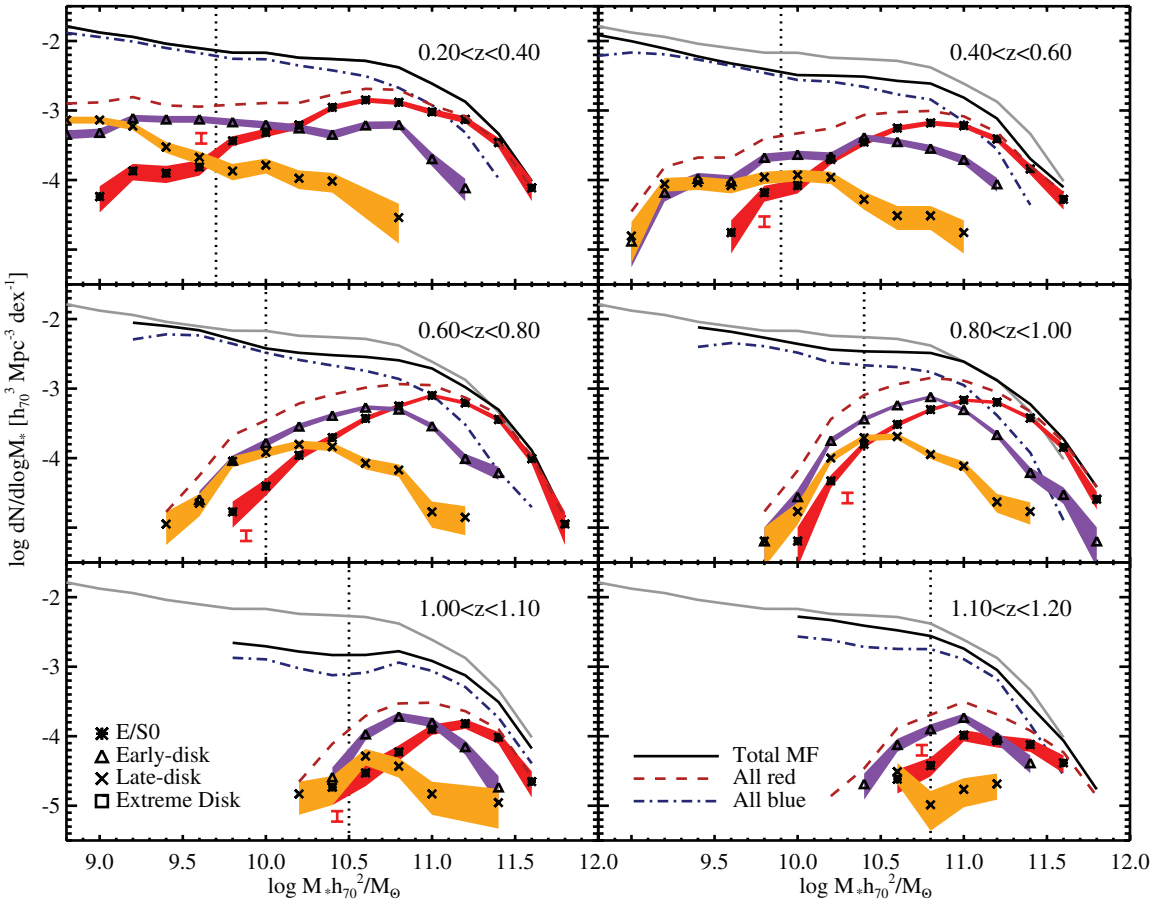

Figure 2. In six redshift intervals, mass functions of galaxies on the red sequence divided by morphological type. The total mass function is shown by the solid black line (the lowest redshift mass function is repeated as a gray line in all panels) while the abundance of passive galaxies (of all types) is shown as the dashed red line and that of star-formers with the blue dash-dotted line. The passive (red-sequence) mass functions are further divided by morphological type as shown by the shaded regions which indicate the 1σ uncertainties. Passive E/S0s have red shading with asterisks, passive early disks ($1.25 \leqslant \langle n \rangle < 2.5$) have purple shading with triangle symbols, and passive late disks ($0.75 \leqslant \langle n \rangle < 1.25$) have orange shading with X symbols. The isolated error bars indicate the systematic uncertainty associated with a 30% upward correction to the number of ZEST spheroidals potentially misclassified at the faintest magnitudes. The contributions from irregulars and passive galaxies with extreme disks (which are very rare) are not shown for clarity. Cosmic variance tends to affect the abundances of sub-populations to a similar degree and introduces differences between redshift panels that can be as large as a factor of 4 but are typically closer to 60%.

(A color version of this figure is available in the online journal.)

prominent disk components (lower $\langle n \rangle$) are more common at lower masses ($\lesssim 10^{10}\ M_{\odot}$) becoming comparable to the more bulge-dominated early disks with higher $\langle n \rangle$ values. On the other hand, these early disks are more frequent at higher masses and there is a redshift-dependent mass range (near $\sim 10^{11} M_{\odot}$) where they are roughly as abundant as passive spheroidals. This general behavior seems to mirror the broader pattern seen when the total population, regardless of rest-frame color, is split by morphological type (e.g., Bundy et al. 2005; Ilbert et al. 2009).

The evolution of morphologies on the red sequence is most easily seen in Figure 3 where the fraction of passive galaxies with a given morphology is plotted as a function of redshift in four M_* bins. While spheroidals dominate the highest masses of the red sequence at all times, at lower masses they start off as a small fraction of passive galaxies at early epochs and rise in importance with time. Meanwhile, the fraction of early and late passive disks tends to decline with time. As we discuss below, it seems plausible from Figure 3 that the passive disks' fraction declines because they transform into passive spheroidals, but Figure 2 shows that their absolute numbers evolve less strongly. It is therefore likely that some star-forming systems (including star-forming spheroidals) transform directly into passive spheroidals. This is supported by Figure 3, which shows that at every redshift, there is an ample supply of star-forming galaxies which may later transform into passive spheroidals.

4.2. Verification of the Passive Disk Population

Figures 2 and 3 reveal a surprisingly abundant population of passive galaxies that appear to contain disk components. As we argue in Section 5, these galaxies offer valuable clues to the mechanisms driving galaxy evolution. We have visually inspected early and late passive disks identified by ZEST in COSMOS and present random examples drawn from specific redshift and M_* ranges in Figures 4 and 5. Early disks tend to be bulge-dominated as expected, with many examples that might be classified as Sa/S0 galaxies. These galaxies often show rounded central regions surrounded by lower surface brightness material that we attribute to the disk component responsible for the relatively low Sérsic values ($1.25 < \langle n \rangle < 2.5$). Note that our choice of ZEST classifications groups objects exhibiting even higher n values ($\langle n \rangle > 2.5$) in the spheroidals category. The late disks (Figure 5) tend to be more elongated with smaller bulges and comparably brighter disk components. In either category and across the full redshift range, there is little evidence for the presence of significant amounts of dust and only a small degree

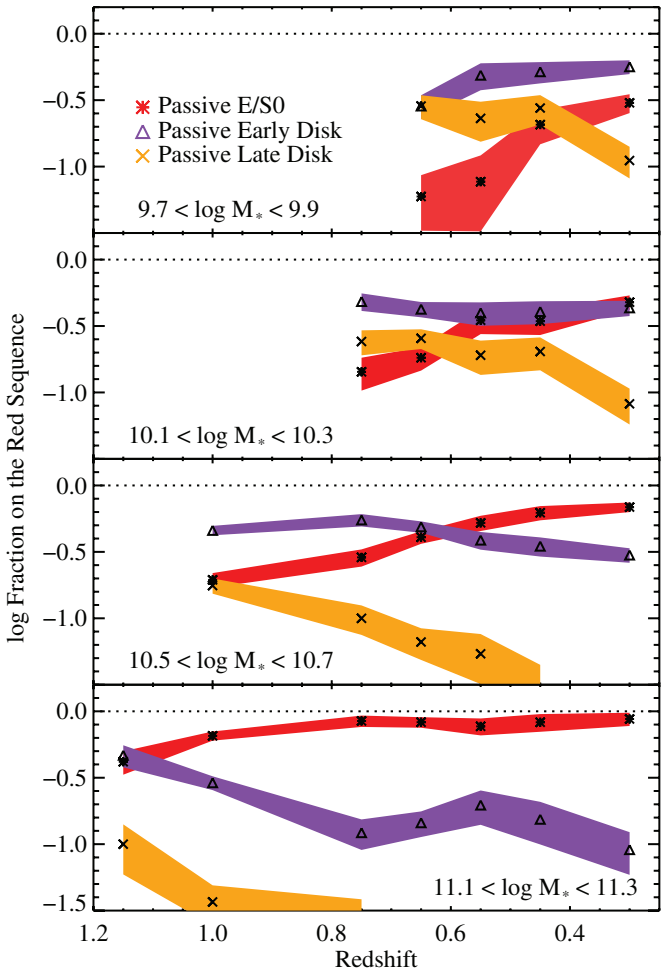

Figure 3. In 4 M_* intervals, the fractional contribution to all red-sequence (passive) galaxies from E/S0s, early-type disks, and late-type disks as a function of redshift. The contribution from irregulars is not shown for clarity. Only data points above the 50% completeness limit for obtaining successful morphological classification are plotted.

(A color version of this figure is available in the online journal.)

of spiral structure. Compared to the clumpier appearance of star-forming disks with spiral arms and associated star-forming regions, the morphology of passive disk galaxies is consistent with the notion that star formation has been largely shut down in these systems.

While direct inspection supports the automated ZEST classifications, systematic biases could remain. In Section 3.4, we discuss how at faint magnitudes ZEST may misclassify up to 30% of spheroidals as disks. This potential bias is illustrated by the systematic error bar in Figure 2 which shows that passive disks would still dominate the low-mass end, even if the maximum 30% correction were applied. We have explored this bias further by comparing the ellipticity distributions of passive and star-forming disks. At the mass completeness limits of our analysis, the ellipticities of passive and star-forming early disks are similar, but late passive disks are weighted toward lower ellipticities. This occurs at a level that is consistent with the expected 30% contamination of the late disk sample by misclassified early disks and spheroidals. Thus, at the mass completeness limits and below, the passive late disk abundance should be viewed with caution given that as much as 30% could be misclassified.

We emphasize, however, that the basic trends in our results are robust because they are still present when we limit our sample to bright magnitudes ($i_{814W} < 22.5$) where the classifications are highly secure. In absolute terms, we see by comparing to Ilbert et al. (2010) that other automated methods classify some fraction of ZEST disks as spheroidals. This is expected given that broad divisions are somewhat arbitrary and that our goal is to identify evidence for disk components even in bulge-dominated galaxies that might otherwise be grouped with spheroidals. The galaxies with disk morphologies in our sample are associated with average Sérsic indices of $\langle n \rangle < 2.5$ for the early disks and $\langle n \rangle < 1.25$ for late disks. A value of $n = 2.5$ has often been used to divide disks from spheroidals (e.g., Barden et al. 2005). However, we should note that surface brightness dimming at high redshifts may make some disk galaxies appear more bulge-dominated, although this works in the opposite sense as the estimated bias at faint magnitudes from Scarlata et al. (2007b). So, until verification through bulge-to-disk decompositions is performed, a conservative interpretation would be to view the abundance of ZEST disks as an upper limit.

A more specific issue is a possible bias from inclination. We expect any type of disk component to be more easily identified in edge-on systems where flatter isophotes are easier to distinguish. Of particular concern is the possibility that dust contamination in edge-on systems could hide residual star formation given that the integrated colors could be dominated by a quiescent bulge. To check this, we have recomputed the mass functions of passive galaxies with the requirement that all galaxies have a ZEST ellipticity class of 0, corresponding to completely face-on systems. This reduces the sample size by ∼80%. While the mass functions shift a bit under this assumption, the essential behavior captured in Figure 3 is unchanged, with the same relative abundance and mass dependence of the various morphological types preserved. We can even compute mass functions requiring significant elongation (ellipticity class 3). While this disfavors spheroidals because they are intrinsically rounder and boosts late disks which are intrinsically flatter, the basic mass and redshift trends are still unchanged. We can therefore rule out an inclination bias in our ability to identify passive disks.

Another concern is the morphological K-correction which could mimic the rising abundance of passive disks at early times if, as expected, galaxies appear more disk-dominated at bluer rest-frame wavelengths. Over the redshift range of the sample ($0.2 < z < 1.2$) the ACS i_{814W} filter corresponds to a rest-frame wavelength range of 4000–6700 Å. It has been shown that morphological K-corrections within this range are small for most galaxies (e.g., Lotz et al. 2004; Cassata et al. 2005), but with only one band of ACS data, it is hard to test this effect directly. Capak et al. (2007a) use a subsample of COSMOS galaxies to show that automated estimators are generally robust to K-corrections, but to address this problem further and check our ZEST-based results more generally, we use the visually classified morphologies in the northern GOODS-N (Giavalisco et al. 2004) as presented in Bundy et al. (2005). These observations have a comparable depth as the COSMOS i_{814W} imaging, but include four *HST*/ACS bands ($BViz$), enabling morphological classifications robust to potential K-corrections.

We identify quiescent stellar populations using similar color–color cuts for the GOODS data as for COSMOS and do indeed find a population of passive disks with *visual* morphological types of Sa–Scd. Figure 6 shows several examples. While the small size of the GOODS comparison sample prevents a detailed comparison, it nonetheless shows similar evidence for an increasing fraction of passive disks as a function of redshift. For $0.4 < z < 0.7$ and above the completeness

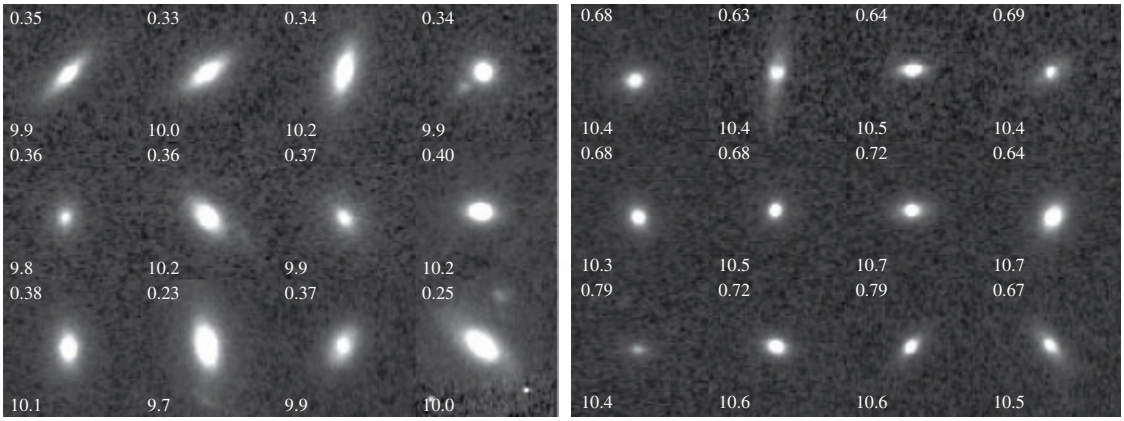

Figure 4. Examples of passive early disks identified using ZEST in the COSMOS data. The left-hand panel shows galaxies with $0.2 < z < 0.4$ and $9.7 < \log M_*/M_\odot < 10.2$ while the right-hand panel corresponds to $0.6 < z < 0.8$ and $10.2 < \log M_*/M_\odot < 10.7$. This class features bulge-dominated systems with average single-Sérsic n values of $1.25 < \langle n \rangle < 2.5$. The galaxies displayed were chosen at random from the subsample. Their redshifts are indicated in the upper left of each postage stamp, the M_* values in $\log M_\odot$ units in the lower left. Each panel is 3″ across, corresponding to roughly 12 kpc at $z \approx 0.3$ and 21 kpc at $z \approx 0.7$.

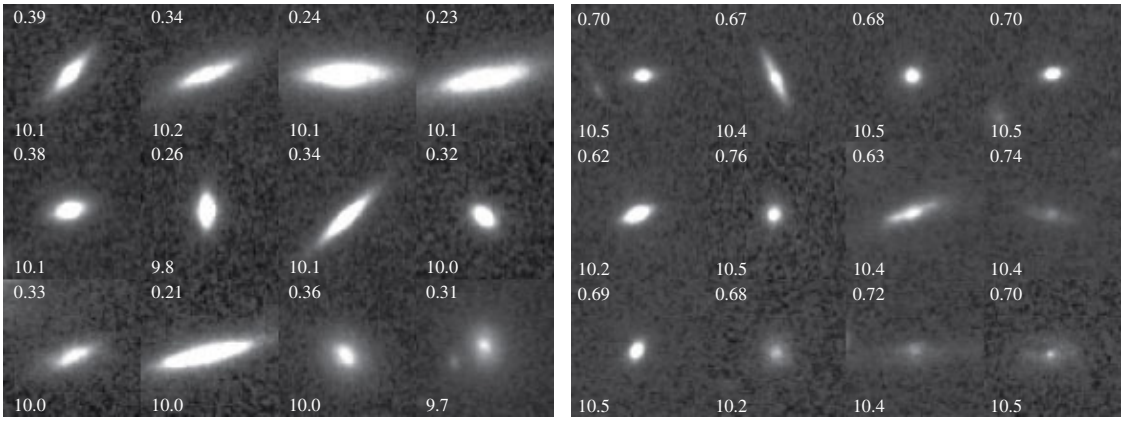

Figure 5. Examples of passive late disks with the two panels corresponding to the same mass and redshift range as in Figure 4. These objects have average Sérsic n values of $0.75 < \langle n \rangle < 1.25$ and are more disk-dominated than the early disks. The postage stamp sizes and labeling is the same as in Figure 4.

limit of $\log M_*/M_\odot \approx 10.2$ we find $\lesssim$20% of the quiescent population is identified as disk-like. At $1.0 < z < 1.1$ and $\log M_*/M_\odot \gtrsim 10.7$, the fraction rises to roughly 35%. While the statistical uncertainty is large, the sense of this trend reinforces the results of the larger COSMOS sample. It should be noted that biases among visual morphologies favor early-type classifications at faint magnitudes and high redshifts due to surface brightness dimming (e.g., Brinchmann et al. 1998). We also note that the GOODS objects show no apparent bias with inclination, in agreement with the inclination tests above. The use of color information in refining the GOODS morphologies indicates that the evolutionary signal is not likely to result from K-corrections and the fact that passive disks identified visually exhibit similar abundances and evolution lends support to the ZEST classifications.

5. DISCUSSION

We have used automated i_{814W}-band ACS morphologies in the COSMOS survey supported by visual morphological classifications of $BViz$ ACS imaging in GOODS-N to argue for the existence of a significant population of passive, bulge-dominated galaxies hosting disk components. These galaxies were more abundant in the past ($z \sim 1$) and are seen to be more common among galaxies with lower M_* at all redshifts probed. In fact, at the low-mass end they represent as much as 70%–90% of the red sequence, even after dusty star-forming red galaxies are removed. At these masses, passive disks account for about 10% of all galaxies. The fact that their abundance depends on both M_* and redshift, and that these dependences are influenced by the strength of the disk component, argues that passive disks hold clues to understanding both the quenching of star formation and morphological evolution within the galaxy population more broadly. We begin our discussion with an assessment of how important passive disks are to galaxy evolution, finding that as many as 60% of galaxies transitioning onto the red sequence may evolve through a passive disk phase. We then discuss possible formation mechanisms, first ruling out simple fading of star-forming disks and strong environmental processes and then moving on to discuss disks regrown in mergers and the suggestion that quenching is initiated by internal structural changes. While no current model fully reproduces the observations at present, our constraints will help refine proposed quenching mechanisms and indicate that morphological and color transformations in galaxies proceed in multiple and sometimes separate stages.

5.1. The Importance of Passive Disks as a Phase of Evolution

How significant are passive disks in the evolutionary history of galaxies? Ideally, we could answer this question by tracking the mass-dependent flow of galaxies transitioning through different evolutionary phases, but unfortunately, as discussed

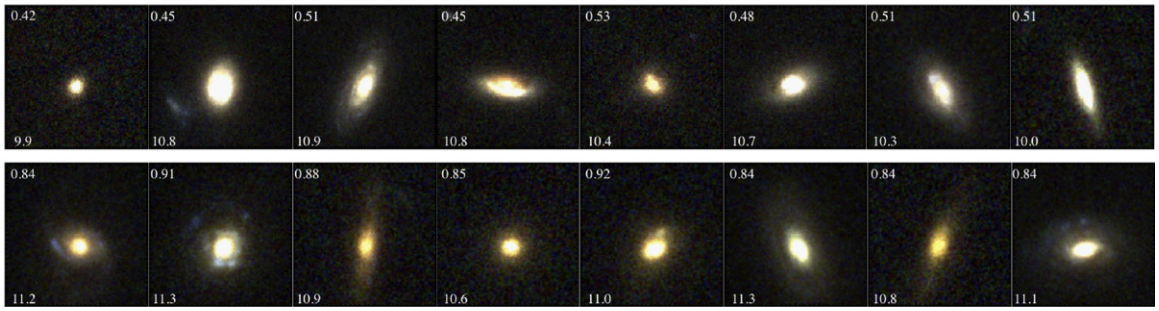

Figure 6. *Viz* color images of passive galaxies in GOODS-N with *visually* classified disk morphologies. The upper strip of eight postage stamps has $0.4 < z < 0.6$ while the lower panel corresponds to $0.8 < z < 1.0$. As in Figure 4, the width of each stamp is $3''$ and redshift is indicated in the upper left, $\log M_*/M_\odot$ in the lower left.

(A color version of this figure is available in the online journal.)

in Section 2.2.1, the strong cosmic variance uncertainties in the single COSMOS field prevent a detailed treatment. Broadly speaking, Figures 2 and 3 in conjunction with previous work suggest that passive disks may represent a significant and relatively common phase of evolution. While the red-sequence abundance grows with time (e.g., Bundy et al. 2006; Borch et al. 2006), passive disks always dominate at lower masses which is also where the newest arrivals to the red sequence can be found (e.g., Treu et al. 2006). This suggests that a large fraction of these quenching galaxies experience an initial passive disk phase. This is supported by Figure 2 which shows that, as with red-sequence spheroidals, the absolute number density of passive disks below $\sim 10^{11} M_\odot$ *increases* with time, even though, compared to all passive galaxies in this mass range, their fraction *decreases* with time. Choosing a mass between 10^{10} and $10^{11} M_\odot$ and comparing the highest and lowest redshifts sampled, we see that ~20%–40% of new red-sequence galaxies formed over this interval can be accounted for by the increase in the number of passive disks. At masses above $\sim 10^{11} M_\odot$, evolution in the absolute abundance of passive disks is more difficult to discern but, as with their fraction, likely declines by 20%–50% (compare the two lower redshift bins in Figure 2 and note the lack of high-mass examples at late times). This reinforces the visual impression of Figure 3, namely, that passive disks evolve into spheroidals. Indeed, as we discuss below, one expects morphological evolution of passive disks to be enhanced compared to their star-forming counterparts because lower gas fractions ($f_{\rm gas}$) enable more minor and, hence, more frequent mergers to drive transformations (Hopkins et al. 2009a). If we make the assumption that all passive disks transform into spheroidals within 1–2 Gyr (e.g., van Dokkum et al. 2005), the fraction of new arrivals to the red-sequence transitioning through a disk phase must increase to compensate, and could be as high as 60%.[17] Passive disk galaxies may therefore represent a fairly common phenomenon and highlight the importance of further morphological evolution along the red sequence.

5.2. Can Passive Disks Form from Faded Star-forming Disks?

At all times, there are as many if not more star-forming disks than passive disks, so it is easy to imagine that passive disks may be drawn from the star-forming population with one important caveat: there are almost no passive galaxies with "extreme disk" (Sérsic $\langle n \rangle < 0.75$) morphologies. Such extreme disks are common in large numbers among star-forming galaxies at all masses and even dominate at the lowest masses where passive disks are most abundant. They would be easily detected if they existed in the passive population. Therefore, the transformation to the red sequence either leads to the formation of a bulge component (e.g., Domínguez-Palmero & Balcells 2009) or requires the existence of one. In the latter case, star-forming and passive disks with similar bulge components should differ only in color but not in their intrinsic structure. We will postpone a detailed comparison of bulge/disk decompositions, scale lengths, and M/L evolution to future work and focus here on a simple comparison of the concentration ($C = R_{80\%}/R_{20\%}$) of passive and star-forming early disks (Figure 7). We consider the nearest redshift bin $0.2 < z < 0.4$ so that the ACS i_{814W} band probes the reddest possible wavelengths (least affected by star formation), and consider the mass range of $9.7 < \log M_*/M_\odot < 10.2$. Passive disks appear to be moderately more concentrated with a peak at $C \approx 3.9$ compared to blue disks with a peak of $C \approx 3.6$ (a Kolmogorov–Smirnov probability test shows that the probability of 0.02 for the distributions being drawn from the same sample). Even after dividing the star-forming disks into low and high SFR subsamples (based on their NUV luminosities) and comparing just the low SFR star-formers to passive disks, this difference in concentration remains. It also holds to $z \approx 0.9$ despite rest-frame morphologies that sample bluer wavelengths. Still, this signature could largely be driven by differences in M/L gradients between star-forming and passive systems. Given this tentative result and the stronger requirement that passive disks be more bulge-dominated than star-forming disks, it seems unlikely that passive disks form simply via the quenching and fading of star formation disk galaxies.

5.3. The Role of Environment

Could passive disks be a product of dense environments? Their morphologies are sometimes reminiscent of S0 galaxies (see Figure 6) that are thought to become increasingly common in clusters (e.g., Dressler et al. 1997; Smith et al. 2005) although recent work disputes this (Holden et al. 2009). While we have specifically attempted to exclude S0s from our disk sample (they are classified as spheroidals), distinguishing them at distant epochs remains difficult (e.g., Moran et al. 2007b). A more promising link exists with "passive spirals" (defined via far UV and spectra line diagnostics) which likely transform into S0s in cluster environments (Moran et al. 2005, 2006, 2007a).

[17] For a mass between 10^{10} and $10^{11} M_\odot$ this percentage can be estimated by assuming that all of the passive disks at $z \approx 1$ become passive spheroidals by $z \approx 0.7$ (an interval of roughly 1.5 Gyr). The remaining spheroidals that have formed between these two redshifts therefore originate from star-forming galaxies. This accounts for ~40% of the total growth of the red-sequence abundance over this interval. Thus, ~60% of red-sequence growth must take the form of passive disks.

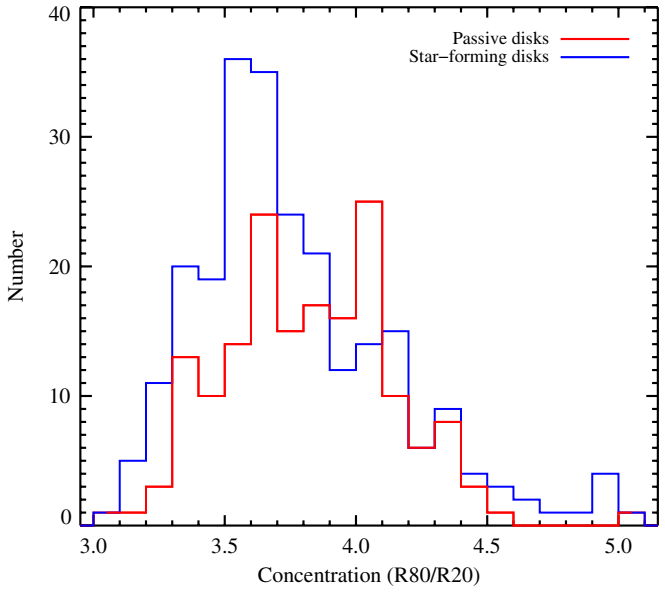

Figure 7. Concentration of passive vs. blue disks of comparable morphologies in the $0.2 < z < 0.4$ redshift range with $9.7 < \log M/M_{\odot} < 10.2$. Passive disks in the same morphological class show evidence of higher concentrations. The ACS i_{814W} band samples the rest frame at ∼6200 Å, thus avoiding potential classification biases owing to star-forming regions.

(A color version of this figure is available in the online journal.)

This transformation process is thought to begin slowly (1–2 Gyr timescales) in infalling groups, perhaps as a result of "gentle" interactions with other galaxies and the intergroup medium. If the intracluster medium (ICM) is sufficiently dense, ram pressure stripping strongly accelerates the quenching of star formation, producing S0s and ellipticals closer to the cluster core and driving evolution in the morphology–density relation (e.g., Capak et al. 2007a).

Because there are only 1–2 clusters in the 1.6 deg^2 COSMOS field (Meneux et al. 2009), cluster mechanisms cannot fully account for the passive disk population studied here. Still, group scale environments may play an important role (see Wilman et al. 2009). To investigate further, we define a "field" sample by removing sources along the line of sight to dense structures. These were identified in the X-ray-selected COSMOS group catalog assembled by Finoguenov et al. (2007) and Leauthaud et al. (2010) which contains 206 groups with weak-lensing calibrated virial (total) masses complete to $M_{200} \approx 3 \times 10^{13} M_{\odot}$ to $z = 0.5$ and $M_{200} \approx 3 \times 10^{14}\, M_{\odot}$ to $z = 1.0$. Any galaxy within the projected R_{200} virial radius of any group, regardless of its redshift, is removed from the field sample, reducing the full sample by ≈30%. Remarkably, the mass dependence and evolution of passive galaxy morphologies (Figure 3) in this field sample is virtually identical to the full sample. This is not to say that there are no environmental trends in the passive disk fraction which would be expected from previous studies of morphology–density relation. Our "field" test simply shows that a large fraction of passive disks live and evolve in halos less massive than $10^{13} M_{\odot}$ (given our two lowest z-bins), ruling out environmental processes in more massive halos as the *sole* explanation.

Even at $M_{200} \approx 10^{13} M_{\odot}$ environmental effects can be important as very weak ram pressure (2–3 orders of magnitude weaker than in cluster cores) can cause "strangulation" or "starvation" via stripping of the galaxy's hot gas halo, thereby shutting off a potential fuel source for subsequent star formation (see McCarthy et al. 2008; Bekki 2009). The starvation scenario would help explain the prevalence of passive disks at low masses, since simulations show that lower mass galaxies are more easily affected. But the starved remnants should have structural properties similar to star-forming disks, a result that seems to be at odds with Figure 7. In addition, McCarthy et al. (2008) show that less concentrated disks are more susceptible to starvation. Yet, the very low concentration "extreme disk" morphologies found in the star-forming population are almost completely absent among passive galaxies. Furthermore, because as M_* increases starvation becomes less effective, we would expect the least concentrated passive disks (the "late types") to occur at the highest masses. Our observations show the opposite trend. We also might expect the group abundance and typical gas density, $n_{\rm ICM}$, to grow with time from $z = 1.5$ (e.g., McGee et al. 2009). Yet, the most massive examples of passive disks, for which $n_{\rm ICM}$ must be large to induce starvation, occur in our *highest* redshift bins ($z \sim 1$).

We therefore conclude that while it is possible that passive disks are a product of low-mass group environments, proposed environmental processes at these scales appear to have some difficulty explaining the observed mass dependence, evolution, and concentration of these galaxies.

5.4. Gas-rich Mergers, Disk Regrowth, and AGN Quenching

Beyond environmental processes, star formation quenching has often been associated with feedback mechanisms triggered by major mergers (e.g., Hopkins et al. 2008). The existence of passive disks presents a problem for this hypothesis: how can a major merger shut down star formation in these galaxies without destroying the underlying stellar disk? One possible solution is that before quenching completes, an entirely new disk is formed (Hammer et al. 2005). Recent high-resolution merger simulations have illustrated exactly this effect (Springel & Hernquist 2005; Robertson et al. 2006; Governato et al. 2009). Roughly speaking, new gaseous disks can form in gas-rich mergers with $f_{\rm gas} > 0.5$ because a lack of central instabilities prevents gas transport to the center and suppresses bulge growth. Given observations of $f_{\rm gas}$ as a function of M_*, mergers with $M_* \approx 10^{10} M_{\odot}$ are much more likely to result in a remnant with a disk-like morphology than similar mergers at $M_* \approx 10^{11} M_{\odot}$ (see Hopkins et al. 2009a).

One of the key aspects of the merger/regrowth model is that the strength of the remnant disk component depends on $f_{\rm gas}$ (Stewart et al. 2009b; Hopkins et al. 2009b). To investigate how predictions from this model compare to our observations, we used the relationships between $f_{\rm gas}$, merger mass ratio (μ), M_*, and remnant bulge-to-total ratio (B/T) that Hopkins et al. (2009a) derive based on a large suite of merger simulations. We assume a scatter of 0.25 dex in the predicted B/T and consider mergers with $0.3 < \mu < 1.0$. We use $f_{\rm gas}(M_*)$ evaluated at $z = 2$ to correspond to passive disk progenitors at $z \sim 1$, and assume that the $z = 0$ relation applies adequately to progenitors at $z \sim 0.3$. Remnant disks are those with $B/T < 0.6$. The results of this exercise are plotted in Figure 8 as two shaded regions for the two redshifts evaluated. These regions represent the predicted disk fractions spanned by mergers of different mass ratios. The region corresponding to the $z = 0$ $f_{\rm gas}(M_*)$ is offset to lower M_*, reflecting the decline of $f_{\rm gas}$ at higher masses. Overplotted are the observed fractions of passive disks (early + late disks) at the two redshifts considered. While in detail, the scatter in predicted B/T likely depends on mass ratio and $f_{\rm gas}$, this toy remnant model does a good job matching

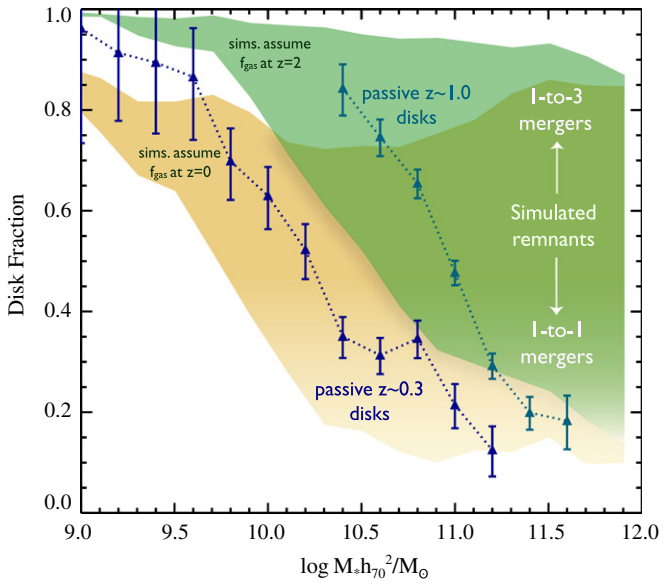

Figure 8. Comparison of the predicted fraction of simulated merger remnants that would be classified as disks to the observed fraction of red-sequence galaxies with disk morphologies (early + late types). The shaded regions denote predictions for two redshift ranges, $z \sim 1$ and $z \sim 0.3$. In either case, low mass ratio mergers predict a high abundance of remnant disks while one-to-one mergers trace the decreasing amount f_{gas} as a function of M_*. Overplotted are the observed passive disk fractions in the two z-bins. The toy model matches the observed passive disk fractions, as well as their mass and redshift dependence, if most formed in mergers with $\mu \sim 1.0$.

(A color version of this figure is available in the online journal.)

the observed passive disk fractions as well as their mass and redshift dependence if most formed in mergers with $\mu \sim 1.0$. A more detailed comparison between predicted and observed morphologies is needed to test this further.

This merger/regrowth scenario is consistent with the lack of a strong environmental dependence (Section 5.3) and would predict that some passive disks will be isolated. This could be tested through clustering and pair count studies. Furthermore, the somewhat higher concentration in passive disks compared to star-formers is naturally explained by the extra bulge mass added during the merger. The big drawback remains understanding how mergers lead to the quenching of star formation. If quenching is short-lived and violent, as in models employing a quasar phase (e.g., Menci et al. 2006; Hopkins et al. 2008), it must somehow be delayed until enough time passes for a stellar disk to regrow (at least 1 Gyr). At the same time, recent simulations have cast doubt on the ability of quasar-mode AGN feedback to directly quench star formation (e.g., DeBuhr et al. 2010).

Instead AGN may be responsible for subtle feedback cycles that prevent gas cooling on longer timescales (1–2 Gyr) after the cold gas is depleted (e.g., Croton et al. 2006). If this feedback is tied to the central black hole mass, this could explain why passive disks have large bulges (Section 5.2), but it does not make clear why other star-forming disk galaxies with similar bulges have not been quenched (Figure 7). Finally, if quenching is initiated by low luminosity AGN feedback, are mergers even required (e.g., Ciotti & Ostriker 2007)? While the specific quenching process in these scenarios remains unknown, the agreement in Figure 8 nevertheless supports a formation mechanism in which the frequency and appearance of passive disks is strongly linked to their progenitor gas fractions.

5.5. A Two Stage Scenario for Morphological Evolution

If star formation in passive disks is shut down because the gas supply is depleted, simulations show that such gas-poor disks can be more easily disrupted by mergers with lower mass ratios—that is, more minor interactions—than disks with high f_{gas}, owing to the ability of gas to regrow disks and suppress bulge formation (Hopkins et al. 2009a). This suggests a two-step process where first, late-type star-forming disks are quenched and transformed into bulge-dominated, passive disks. This makes them vulnerable to minor interactions that, second, disrupt the disk component and convert them into spheroidals.[18]

Figure 2 suggests that this two-step evolution may have a broad impact on interpretations of how morphological populations evolve. The figure shows that passive disks account for as much as one-third of all disk galaxies at $M_* \sim 10^{11} M_\odot$ while the number declines toward lower masses (and redshifts). Assuming they are gas-poor and susceptible to more minor interactions, then because minor mergers are far more common than major mergers (e.g., Stewart et al. 2009a), this passive one-third of the disk population is likely to account for many of the newly formed spheroidals since $z \sim 1$ (e.g., Bundy et al. 2005; Ilbert et al. 2010). But recent efforts to compare the formation rate of spheroidals to the merger rate have focused only on rarer, *major* mergers, assuming perhaps incorrectly that single mergers of gas-rich disks are the only channel for spheroidal formation (e.g., Bundy et al. 2007; Genel et al. 2008; Bundy et al. 2009). These studies have suggested that the major merger rate, both as observed and predicted, may be 2–3 times too low to explain the formation of new spheroidals. While a more precise comparison requires consistency in defining mass ratios, morphologies, and understanding gas effects (Hopkins et al. 2010), including more prevalent minor mergers involving passive disks could help bring current measures of the two phenomena into better agreement.

5.6. Morphological Quenching

The environmental effects and merger/regrowth model we have considered depend on phenomena that are external to the galaxy. It is also possible that passive disks form as a result of *internal* processes. An example of this is "morphological quenching" (MQ; Martig et al. 2009). In this model, after the cold streams that fuel high-z star formation shut down or become clumpy (Dekel et al. 2009), the further fragmentation of gaseous disks—and therefore its ability to form stars—can be internally suppressed by two processes. The first is the declining self-gravity of the gas as it is converted to stars and the second is the deepening central potential caused by stellar bulge growth resulting from instabilities in the stellar disk or even minor mergers. The predicted remnants of morphological quenching are consistent with many of our observations. They would appear as passive disks with large bulges, would have a weak environmental dependence, and exhibit slow quenching, in this case initiated by gradual changes in internal structure.

While more detailed comparisons between observations and simulations of morphological quenching (Martig et al. 2009) are clearly needed, we note that many of the examples in Figures 4–6 show large, thick disks. In future work, this may

[18] We avoid the term "dry mergers" here, even though the interactions considered would have low f_{gas}, because dry mergers have come to denote the more narrow concept of nearly binary mergers between gas-poor, but already spheroidal galaxies.

help distinguish between an early formation with thickening from disk instabilities that could accelerate MQ (Bournaud et al. 2009) and later disk regrowth (Hopkins et al. 2009a). It is also important to determine if MQ can explain why bulge growth leads to quenching in some galaxies but not in others as well as why passive disks are more disk-dominated at lower M_* (Figure 2). The higher gas fractions at these masses would naively require larger, not smaller bulges. Finally, we note that morphological quenching requires testable deviations from the Kennicutt–Schmidt relation (e.g., Donovan et al. 2009) and implies that gas disks in passive galaxies remain intact. Subsequent mergers of passive disks in this scenario could therefore produce new star-forming galaxies instead of passive spheroidals.

5.7. Comparison with an SDSS Sample

Finally, while this work has focused on mass-limited samples at high redshift, a detailed study by Masters et al. (2010) of a subset of passive disks identified using GZ in SDSS provides additional insight. A direct comparison is not possible because the GZ passive disks were selected using a single color ($g - r$) and were required to be mainly face-on and to have spiral arms as identified by GZ users. Still, the two samples paint a consistent picture. Red GZ disks are more common at higher masses (see also van der Wel et al. 2009) and tend to host larger bulges than their star-forming counterparts. Their emission lines indicate little ongoing SF but are inconsistent with post-starburst spectra, favoring instead a gradual decline of SF over 1–2 Gyr. They tend to live in intermediate environments consistent with the $\lesssim 10^{13} M_\odot$ halos our observations suggest. More than 75% host nuclear bars and 50%–80% show evidence for LINER emission. Assuming the GZ sample is representative of passive disks in general, the Masters et al. (2010) analysis supports a formation mechanism that is strongly tied to a bulge and a central bar, somewhat weakly tied to environment, and capable of quenching star formation slowly.

6. SUMMARY AND CONCLUSIONS

We have used the COSMOS survey to identify a significant population of non-star-forming, passive disk galaxies and have studied their importance with respect to the growth of the red sequence and the formation of spheroidal galaxies. After removing dusty contaminants, evidence for disk components is found in nearly half of galaxies on the red sequence at all redshifts, primarily at the low-mass end. The absolute number of passive disks below $\sim 10^{11} M_\odot$ appears to increase with time, mirroring the growth of the red sequence, although the number of passive spheroidals increases faster. Above $\sim 10^{11} M_\odot$, the abundance of passive disks has declined since $z \sim 1$. We interpret these trends to indicate that passive disks may be a relatively common phase of galaxies transitioning onto the red sequence, accounting for as much as 60% of newly quenched systems. The declining contribution of passive disks to the red sequence with time suggests that, once formed, they transform into spheroidals on moderately fast (1–3 Gyr) timescales. This is likely aided by the fact that unlike star-forming galaxies, passive disks may be more susceptible to morphological evolution induced by minor mergers, given their depleted gas supply (Hopkins et al. 2009b). Thus, the formation of many red-sequence ellipticals does not occur in a single event like a major merger, and may instead proceed through two or more evolutionary stages.

Understanding how passive disks form can shed light on the physical processes that shape galaxy evolution more broadly. Do passive disks evolve slowly from star-forming disks that exhaust their gas supply after cooling is suppressed or become stabilized to fragmentation? Or, do they form more rapidly after some event, such as a merger or falling into a galaxy group? While more work is needed, early results from this analysis and a study of a subset of passive disks in SDSS (Masters et al. 2010) provide tantalizing clues. First, passive disks are almost exclusively bulge-dominated. Star-forming disks on the other hand include a large number of strongly disk-dominated galaxies at all epochs. A bulge component is either required to shut down star formation—perhaps because a bulge signals the presence of a potential AGN—or is built during the formation process. The presence of a large bulge, however, does not guarantee that star formation is shut down. Beyond this, passive disks with the same mass, redshift, and morphological type are more concentrated on average than star-formers. While these assertions should be verified with stellar mass bulge/disk decompositions, it appears that at least some fraction of passive disks is structurally distinct.

We have used a toy model to show that mergers, which naturally increase bulge mass but can also form a new disk (e.g., Springel & Hernquist 2005), produce remnants with a similar mass and redshift dependence as passive disks. This agreement suggests a strong link between morphology and $f_{\rm gas}$. The problem with the merger/regrowth model remains understanding how the merger induces quenching. SDSS observations of passive disk emission lines favor a slow process (Masters et al. 2010) that operates over 1–2 Gyr. This seems inconsistent with a merger-triggered quasar phase, which must be delayed to allow enough time for a new disk to form. On the other hand, slow quenching may take place in $10^{13} M_\odot$ halos in which the group medium can slowly "starve" galaxies of fuel by stripping their hot gas reservoirs. Environmental processes therefore present an alternative to the merger/regrowth model but have trouble accounting for the importance of bulges and the way in which passive disk morphologies depend on mass and redshift. The newly proposed morphological quenching scenario (Martig et al. 2009) also predicts slow quenching as internal structural changes suppress disk fragmentation and star formation. This mechanism requires large bulges, as observed, and predicts thick stellar disks (Bournaud et al. 2009). More detailed comparisons and a test of the predicted mass and redshift dependences in this scenario are now needed.

The prospects for resolving the formation mechanism look promising and we note that some combination of the processes considered here may be operating simultaneously. More detailed studies of the structure, color gradients, and stellar populations of passive disks will help link them with their progenitors. At the same time, it is important to verify the high disk fractions revealed by the ZEST classifier with bulge-to-disk decompositions, ideally performed in terms of stellar mass. This will confirm the significance of disk components and enable more direct comparisons to star-forming samples as well as simulations. Improvements at low-z will come from expanded, mass-limited samples, and at high-z from clustering and pair-count studies. Larger samples from future surveys will overcome cosmic variance and allow individual populations to be tracked as they evolve through different stages. Both with current surveys and in the future, passive disks offer a unique opportunity to separate and understand the processes that drive global patterns of galaxy evolution since $z \sim 1$.

We thank Eliot Quataert, Arjen van der Wel, Avishai Dekel, Frédéric Bournaud, Bob Nichol, Karen Masters, and Tommaso Treu for very useful discussions and feedback. K.B. acknowledges support for this work provided by NASA through Hubble Fellowship grant HF-01215, awarded by the Space Telescope Science Institute, which is operated by the Association of Universities for Research in Astronomy, Inc., for NASA, under contract NAS 5-26555. We acknowledge the entire COSMOS collaboration which has made this work possible. More information on the COSMOS survey is available at http://www.astro.caltech.edu/cosmos.

REFERENCES

Abraham, R. G., et al. 2007, ApJ, 669, 184
Aune, S., et al. 2003, Proc. SPIE, 4841, 513
Baldry, I. K., Glazebrook, K., Brinkmann, J., Ivezić, Ž., Lupton, R. H., Nichol, R. C., & Szalay, A. S. 2004, ApJ, 600, 681
Balogh, M. L., Baldry, I. K., Nichol, R., Miller, C., Bower, R., & Glazebrook, K. 2004, ApJ, 615, L101
Bamford, S. P., et al. 2009, MNRAS, 393, 1324
Barden, M., et al. 2005, ApJ, 635, 959
Bekki, K. 2009, MNRAS, 399, 2221
Bell, E. F., McIntosh, D. H., Katz, N., & Weinberg, M. D. 2003, ApJS, 149, 289
Bell, E. F., et al. 2004, ApJ, 608, 752
Birnboim, Y., Dekel, A., & Neistein, E. 2007, MNRAS, 380, 339
Blanton, M. R., & Roweis, S. 2007, AJ, 133, 734
Bolzonella, M., et al. 2009, arXiv:0907.0013
Borch, A., et al. 2006, A&A, 453, 869
Boulade, O., et al. 2003, Proc. SPIE, 4841, 72
Bournaud, F., Elmegreen, B. G., & Martig, M. 2009, ApJ, 707, L1
Bower, R. G., et al. 2006, MNRAS, 370, 645
Brand, K., et al. 2009, ApJ, 693, 340
Brinchmann, J., & Ellis, R. S. 2000, ApJ, 536, L77
Brinchmann, J., et al. 1998, ApJ, 499, 112
Brown, M. J. I., et al. 2007, ApJ, 654, 858
Bruzual, G., & Charlot, S. 2003, MNRAS, 344, 1000
Bundy, K., Ellis, R. S., & Conselice, C. J. 2005, ApJ, 625, 621
Bundy, K., Fukugita, M., Ellis, R. S., Targett, T. A., Belli, S., & Kodama, T. 2009, ApJ, 697, 1369
Bundy, K., Treu, T., & Ellis, R. S. 2007, ApJ, 665, L5
Bundy, K., et al. 2006, ApJ, 651, 120
Capak, P., Abraham, R. G., Ellis, R. S., Mobasher, B., Scoville, N., Sheth, K., & Koekemoer, A. 2007a, ApJS, 172, 284
Capak, P., et al. 2007b, ApJS, 172, 99
Cassata, P., et al. 2005, MNRAS, 357, 903
Cassata, P., et al. 2007, ApJS, 172, 270
Cattaneo, A., Dekel, A., Devriendt, J., Guiderdoni, B., & Blaizot, J. 2006, MNRAS, 370, 1651
Cattaneo, A., Dekel, A., Faber, S. M., & Guiderdoni, B. 2008, MNRAS, 389, 567
Chabrier, G. 2003, PASP, 115, 763
Ciotti, L., & Ostriker, J. P. 2007, ApJ, 665, 1038
Conroy, C., Gunn, J. E., & White, M. 2009, ApJ, 699, 486
Conselice, C. J. 2003, ApJS, 147, 1
Cooper, M. C., et al. 2007, MNRAS, 383, 1058
Cowie, L. L., Songaila, A., Hu, E. M., & Cohen, J. G. 1996, AJ, 112, 839
Croton, D. J., et al. 2006, MNRAS, 365, 11
Cucciati, O., et al. 2006, A&A, 458, 39
DeBuhr, J., Quataert, E., Ma, C., & Hopkins, P. 2010, MNRAS, 406, L55
Dekel, A., & Birnboim, Y. 2006, MNRAS, 368, 2
Dekel, A., Sari, R., & Ceverino, D. 2009, ApJ, 703, 785
de Vaucouleurs, G., de Vaucouleurs, A., Corwin, H. G., Jr., Buta, R. J., Paturel, G., & Fouque, P. 1991, Third Reference Catalogue of Bright Galaxies (New York: Springer)
Domínguez-Palmero, L., & Balcells, M. 2009, ApJ, 694, L69
Donovan, J. L., et al. 2009, AJ, 137, 5037
Dressler, A., et al. 1997, ApJ, 490, 577
Drory, N., et al. 2009, ApJ, 707, 1595
Faber, S. M., et al. 2003, Proc. SPIE, 4841, 1657
Ferreras, I., Lisker, T., Pasquali, A., & Kaviraj, S. 2009, MNRAS, 395, 554
Finoguenov, A., et al. 2007, ApJS, 172, 182
Fiore, F., et al. 2008, ApJ, 672, 94
Franceschini, A., et al. 2006, A&A, 453, 397
Frei, Z., Guhathakurta, P., Gunn, J. E., & Tyson, J. A. 1996, AJ, 111, 174
Genel, S., et al. 2008, ApJ, 688, 789
Giavalisco, M., et al. 2004, ApJ, 600, L93
Governato, F., et al. 2009, MNRAS, 398, 312
Hammer, F., Flores, H., Elbaz, D., Zheng, X. Z., Liang, Y. C., & Cesarsky, C. 2005, A&A, 430, 115
Holden, B. P., et al. 2009, ApJ, 693, 617
Hopkins, P. F., Cox, T. J., Kereš, D., & Hernquist, L. 2008, ApJS, 175, 390
Hopkins, P. F., Cox, T. J., Younger, J. D., & Hernquist, L. 2009a, ApJ, 691, 1168
Hopkins, P. F., et al. 2009b, MNRAS, 397, 802
Hopkins, P., et al. 2010, arXiv:1004.2708
Ilbert, O., et al. 2009, ApJ, 690, 1236
Ilbert, O., et al. 2010, ApJ, 709, 644
Juneau, S., et al. 2005, ApJ, 619, L135
Kannappan, S. J., Guie, J. M., & Baker, A. J. 2009, AJ, 138, 579
Kauffmann, G., et al. 2003, MNRAS, 341, 54
Kaviraj, S., Peirani, S., Khochfar, S., Silk, J., & Kay, S. 2009, MNRAS, 394, 1713
Kitzbichler, M. G., & White, S. D. M. 2007, MNRAS, 376, 2
Koekemoer, A. M., et al. 2007, ApJS, 172, 196
Komiyama, Y., et al. 2003, Proc. SPIE, 4841, 152
Labbé, I., et al. 2005, ApJ, 624, L81
Leauthaud, A., et al. 2007, ApJS, 172, 219
Leauthaud, A., et al. 2010, ApJ, 709, 97
Lilly, S. J., et al. 2007, ApJS, 172, 70
Lintott, C. J., et al. 2008, MNRAS, 389, 1179
Lotz, J. M., Primack, J., & Madau, P. 2004, AJ, 128, 163
Maraston, C., et al. 2006, ApJ, 652, 85
Martig, M., Bournaud, F., Teyssier, R., & Dekel, A. 2009, ApJ, 707, 250
Masters, K. L., et al. 2010, MNRAS, 405, 783
McCarthy, I. G., Frenk, C. S., Font, A. S., Lacey, C. G., Bower, R. G., Mitchell, N. L., Balogh, M. L., & Theuns, T. 2008, MNRAS, 383, 593
McCracken, H. J., et al. 2010, ApJ, 708, 202
McGee, S. L., Balogh, M. L., Bower, R. G., Font, A. S., & McCarthy, I. G. 2009, MNRAS, 400, 937
Menci, N., Fontana, A., Giallongo, E., Grazian, A., & Salimbeni, S. 2006, ApJ, 647, 753
Meneux, B., et al. 2009, A&A, 505, 463
Mobasher, B., et al. 2009, ApJ, 690, 1074
Moran, S. M., Ellis, R. S., Treu, T., Salim, S., Rich, R. M., Smith, G. P., & Kneib, J.-P. 2006, ApJ, 641, L97
Moran, S. M., Ellis, R. S., Treu, T., Smail, I., Dressler, A., Coil, A. L., & Smith, G. P. 2005, ApJ, 634, 977
Moran, S. M., Ellis, R. S., Treu, T., Smith, G. P., Rich, R. M., & Smail, I. 2007a, ApJ, 671, 1503
Moran, S. M., Loh, B. L., Ellis, R. S., Treu, T., Bundy, K., & MacArthur, L. A. 2007b, ApJ, 665, 1067
Noeske, K. G., et al. 2007, ApJ, 660, L43
Oesch, P. A., et al. 2010, ApJ, 714, L47
Pannella, M., et al. 2006, ApJ, 639, L1
Pannella, M., et al. 2009, ApJ, 701, 787
Polletta, M., et al. 2007, ApJ, 663, 81
Pozzetti, L., & Mannucci, F. 2000, MNRAS, 317, L17
Pozzetti, L., et al. 2009, arXiv:0907.5416
Puget, P., et al. 2004, Proc. SPIE, 5492, 978
Rieke, G. H., Alonso-Herrero, A., Weiner, B. J., Pérez-González, P. G., Blaylock, M., Donley, J. L., & Marcillac, D. 2009, ApJ, 692, 556
Robertson, B., Bullock, J. S., Cox, T. J., Di Matteo, T., Hernquist, L., Springel, V., & Yoshida, N. 2006, ApJ, 645, 986
Ruhland, C., Bell, E. F., Häußler, B., Taylor, E. N., Barden, M., & McIntosh, D. H. 2009, ApJ, 695, 1058
Sargent, M. T., et al. 2007, ApJS, 172, 434
Scarlata, C., et al. 2007a, ApJS, 172, 406
Scarlata, C., et al. 2007b, ApJS, 172, 494
Schawinski, K., et al. 2009, MNRAS, 396, 818
Schmidt, M. 1968, ApJ, 151, 393
Scoville, N., et al. 2007a, ApJS, 172, 38
Scoville, N., et al. 2007b, ApJS, 172, 1
Smith, G. P., Treu, T., Ellis, R. S., Moran, S. M., & Dressler, A. 2005, ApJ, 620, 78
Somerville, R. S., Hopkins, P. F., Cox, T. J., Robertson, B. E., & Hernquist, L. 2008, MNRAS, 391, 481

Springel, V., & Hernquist, L. 2005, ApJ, 622, L9
Stewart, K. R., Bullock, J. S., Barton, E. J., & Wechsler, R. H. 2009a, ApJ, 702, 1005
Stewart, K. R., Bullock, J. S., Wechsler, R. H., & Maller, A. H. 2009b, ApJ, 702, 307
Stockton, A., McGrath, E., Canalizo, G., Iye, M., & Maihara, T. 2008, ApJ, 672, 146
Stringer, M. J., Benson, A. J., Bundy, K., Ellis, R. S., & Quetin, E. L. 2009, MNRAS, 393, 1127
Tasca, L. A. M., et al. 2009, A&A, 503, 379
Toomre, A. 1977, in Evolution of Galaxies and Stellar Populations, ed. B. M. Tinsley & R. B. Larson (New Haven, CT: Yale Univ. Observatory), 401
Treu, T., Koopmans, L. V., Bolton, A. S., Burles, S., & Moustakas, L. A. 2006, ApJ, 640, 662
van den Bergh, S. 2009, ApJ, 702, 1502
van der Wel, A. 2008, ApJ, 675, L13
van der Wel, A., Rix, H., Holden, B. P., Bell, E. F., & Robaina, A. R. 2009, ApJ, 706, L120
van der Wel, A., et al. 2007, ApJ, 670, 206
van Dokkum, P. G., Kriek, M., Rodgers, B., Franx, M., & Puxley, P. 2005, ApJ, 622, L13
van Dokkum, P. G., et al. 2006, ApJ, 638, L59
Williams, R. J., Quadri, R. F., Franx, M., van Dokkum, P., & Labbé, I. 2009, ApJ, 691, 1879
Willmer, C. N. A., et al. 2006, ApJ, 647, 853
Wilman, D. J., Oemler, A., Mulchaey, J. S., McGee, S. L., Balogh, M. L., & Bower, R. G. 2009, ApJ, 692, 298
Wuyts, S., et al. 2007, ApJ, 655, 51
Yan, R., Newman, J. A., Faber, S. M., Konidaris, N., Koo, D., & Davis, M. 2006, ApJ, 648, 281